Research Paper

THEMED ISSUE: Geothermal Energy from Sedimentary Basins: Challenges, Potential, and Ways Forward

GEOSPHERE

GEOSPHERE; v. 12, no. 4

doi:10.1130/GES01235.1

6 figures; 2 tables

CORRESPONDENCE: dhananjay.ravat@uky.edu

CITATION: Ravat, D., Morgan, P., and Lowry, A.R. 2016, Geotherms from the temperature-depth–constrained solutions of 1-D steady-state heat-flow equation: Geosphere, v. 12, no. 4, p. 1187–1197, doi:10.1130/GES01235.1.

Received 19 July 2015
Revision received 4 March 2016
Accepted 9 May 2016
Published online 16 June 2016

Geotherms from the temperature-depth–constrained solutions of 1-D steady-state heat-flow equation

D. Ravat[1], P. Morgan[2], and A.R. Lowry[3]

[1]Department of Earth and Environmental Sciences, University of Kentucky, Lexington, Kentucky 40506-0053, USA
[2]Colorado Geological Survey, Colorado School of Mines, 1801 19th Street, Golden, Colorado 80401, USA
[3]Department of Geology, Utah State University, Logan, Utah 84322-4505, USA

ABSTRACT

We use the Curie depth derived from spectral analysis of near-surface magnetic anomaly data to constrain the solution of a one-dimensional (1-D) steady-state heat-flow equation. The method, in addition to anchoring the geotherm at deep levels in the crust, yields the ratio of radiogenic heat production to thermal conductivity. We evaluate the utility of this constraint in two granitic regions in the United States where radiogenic heat production, thermal conductivity, and heat flow are well determined. We also examine the results of this method in the context of previous research in the central Red Sea and coastal Saudi Arabia. In a test case using data from New Hampshire, USA, the steady-state approximation applies, and we calculate heat-production values (~8 μW/m³) that agree with measurements on samples of Conway granite in the region. In the second example, our Wyoming geotherm is hotter by ~200 °C at the Curie depth, possibly reflecting the 15 km thicker crust (as observed from the dense EarthScope USArray stations in comparison to only two earlier refraction profiles) and the consequent greater radiogenic heat production in the lower crust. In the Colorado Front Range, our radiogenic heat-production value is somewhat higher than predicted from previous heat-flow studies and may reflect heat advected by intrusions. Our results indicate that basal crustal temperatures in northern Colorado may be close to solidus of rocks of felsic composition, a scenario that is consistent with the geological history of the region and has important implications for crustal rheology. Our estimates of depth-integrated heat production from the crustal columns (25 and 55 mW/m² Wyoming and Colorado, respectively) also agree well with estimates from previous studies.

INTRODUCTION

Solutions of the 1-D steady-state heat-flow equation with different boundary conditions (e.g., heat flow at the surface or the Moho) are commonly used to construct geotherms in the lithosphere in situations where steady-state conductive thermal transfer is assumed (Carslaw and Jaeger, 1986; Fowler, 2005). In addition to heat coming from the mantle, heat produced by decay of radioactive elements, primarily U, Th, and K, in the crust is an important contributor to heat flow at the surface (Clauser, 2011). This is true especially for continental crust where felsic rocks are enriched in the heat-producing radioactive elements (Wollenberg and Smith, 1987). Unless the contribution from radiogenic heat is known from measurements of rocks, it must be estimated, and unless the deep geotherm is constrained petrologically from xenoliths (which may not be representative of present-day temperatures), temperature deep in the crust is largely unconstrained. Where there is no temperature constraint at depth and/or where the assumptions adopted to solve the heat-flow equation are violated, the derived geotherm calculation may misrepresent temperatures deep in the crust.

One parameter needed to estimate the geotherm is radiogenic heat production of the crust. Based on measurements and geochemistry of crustal rocks, the average rate of radiogenic heat production in the upper continental crust is estimated between 2.5 and 2.9 μW/m³. The range for felsic rocks is 0.7–28 with the mean of 4.8 μW/m³ and the range for mafic rocks is 0.04–4.1 with the mean of 0.7 μW/m³ (Wollenberg and Smith, 1987). The continental crust is heterogeneous, however, and in all but a few special geologic terrains (large granitic plutons), surface measurements are not representative of upper crustal radiogenic heat production, and the heat production rate for any specific locality is not known. In this paper, we develop a method to estimate heat production of the crust by applying a constraint of a temperature at depth (specifically, the Curie temperature depth of magnetite inferred from spectral analysis of magnetic data; although other temperature proxies from seismology and electromagnetic methods may be used similarly).

It is well known that the base of magnetization in the lithosphere may be controlled by the phenomenon of Curie temperature of magnetic minerals. Curie temperature, or Curie point, is the temperature above which ferromagnetic materials lose their spontaneous magnetization and become paramagnetic. At depths where the temperature is above the Curie temperature of magnetic minerals, rocks are paramagnetic and do not contribute to magnetic anomalies observed at or above the Earth's surface. This phenomenon has been used in deriving the Curie point depth in several studies since Bhattacharyya and Leu (1975) developed a method for calculating this depth. The magnetization of the crust is often governed by concentrations of magnetite because generally magnetite is more strongly magnetic than most other minerals. Rocks containing hemo-ilmenite or ilmeno-hematite have been shown to carry a significant

amount of natural remanent magnetization (McEnroe and Brown, 2000; Robinson et al., 2002) and will have variable Curie points depending on composition. However, these minerals occur only in certain environments, and, hence, the Curie point of magnetite (580 °C) is generally used to estimate temperatures deeper in the crust from the detected base of magnetization.

Early magnetic depth-determination methods assumed sources and ensembles of sources of uniform magnetization in the crust, and the slopes of the annular-averaged spectra from magnetic anomalies were used to estimate depths to magnetic layers (e.g., Spector and Grant, 1970; Okubo et al., 1985; Tanaka et al., 1999). In the 1990s, researchers recognized that the crustal magnetization may be fractal in its distribution (Maus and Dimri, 1994, 1995; Pilkington and Todoeschuck, 1995). A fractal distribution introduces a power-law dependence into magnetic spectra (Pilkington and Todoeschuck, 1993). Without correction for the fractal effect, the depths to magnetic layers and the magnetic bottom can be overestimated. In determining magnetic bottom depth, Ross et al. (2006) and Ravat et al. (2007) introduced the method of forward modeling the spectral peak caused by the bottom of the magnetic layer. However, most magnetic spectra do not form spectral peaks; the lack of a peak is considered to reflect fractal behavior of the magnetic anomaly field and fractal behavior of magnetization. Around this time, methods that consider the fractal nature of crustal magnetization were introduced in magnetic depth-estimation methods (Maus and Dimri, 1996; Maus et al., 1997; Ravat et al., 2007; Bouligand et al., 2009; Bansal et al., 2011). However, until Salem et al. (2014) introduced the de-fractal method, it was not possible to estimate the fractal parameter of the magnetic field needed in applying the correction. Most researchers use a fixed value to determine magnetic bottom depths (e.g., Bouligand et al., 2009; Bansal et al., 2011, 2013; Li et al., 2013); however, the a priori fixed fractal parameter gives correct depths only when the chosen fractal parameter is correct (and if spectral slopes are picked correctly). The method will under- or over-estimate depths if the chosen fractal parameter is higher or lower, respectively. The de-fractal method of Salem et al. (2014) compensates for the fractal parameter of the magnetic anomaly field such that a spectral peak is formed, which then can be modeled using forward-modeling techniques (Ross et al., 2006; Ravat et al., 2007). The de-fractal method also uses the consistency of results from both the centroid method (Okubo et al., 1985; Tanaka et al., 1999; Bansal et al., 2011) and the peak modeling method to identify the fractal correction parameter. The 2-D de-fractal method (where magnetization variation is in the xy-plane and magnetization is constant in depth) is developed and tested in detail by Salem et al. (2014). We modified the procedure of Salem et al. (2014) and made it semi-automatic for the purpose of testing additional feasible interpretations. The details of the procedure and relevant model study results are given in Appendix A.

In this paper, we use magnetic bottom depths derived from the de-fractal method and the Curie temperature of magnetite as a temperature-depth constraint in the solution of a 1-D steady-state heat-flow equation. We find that the constraint allows us also to estimate the bulk radiogenic heat production. This analysis assumes an exponential distribution of heat production in the crust, and justification for this assumption is given in Appendix B. We test this method in two areas in the United States with well-constrained surface heat-flow and radiogenic heat-production data; we also reassess our previous results in the Red Sea region and in coastal Saudi Arabia (Salem et al., 2014).

Geotherm Using the Curie-Depth Constraint

We assume a linear relationship of surface heat flow to heat production (Birch et al., 1968; Roy et al., 1968):

$$q_s = q_r + A_s b,$$

where q_s is surface heat flow, q_r is reduced heat flow, A_s is surface heat production, and b is the empirical heat-production depth-distribution parameter. The linear relationship is consistent with an exponential depth distribution of heat production (Lachenbruch, 1968):

$$A_z = A_s \exp(-z/b) \text{ for all depths, z.}$$

The linear relation and exponential distribution were introduced for terrains dominated by granitic plutons, and we apply them in the same types of terrains in this paper. The exponential distribution has been challenged, and in Appendix B, we discuss data that have been used to question its validity. This distribution is used in the present study only for terrains dominated by granitic plutons.

Assuming as boundary conditions,

(i) $T = T_s$ at $z = 0$ (the surface), where T is temperature, z is depth, and

(ii) $q = -K\,\mathrm{d}T/\mathrm{d}z = -q_s$ at $z = 0$, where K is thermal conductivity, q is heat flow, and q_s is the surface heat flow and neglecting contributions from mass advection, transient cooling or temperature dependence of thermal conductivity, the solution of the 1-D heat-flow equation is:

$$T_z = T_s + \frac{q_s z}{K} + \frac{A_s b(b-z)}{K} - \frac{A_s b^2 \exp(-z/b)}{K} \text{ for all } z. \quad (1)$$

We add an a posteriori condition to Equation 1: $T = T_c$ at $z = z_c$, where T_c is the Curie temperature and z_c is the Curie depth.

We restrict the application of this technique to provinces dominated by granitic plutons from which a mean q_s and b are known. Using $q_s = K\left(\frac{\mathrm{d}T}{\mathrm{d}Z}\right)_{z=0}$, Equation 1 becomes

$$T_c - T_s = +\frac{q_s}{K} z_c + \frac{A_s b(b-z_c)}{K} - \frac{A_s b^2 \exp(-z_c/b)}{K}$$

$$\therefore K\left[(T_c - T_s) - \frac{\mathrm{d}T}{\mathrm{d}Z_{(z=0)}} z_c\right] = A_s b[b - z_c - b\exp(-z_c/b)]$$

$$\therefore \frac{A_s}{K} = \left(\frac{(T_c - T_s) - \left(\frac{\mathrm{d}T}{\mathrm{d}Z}\right)_{z=0} z_c}{b[b - z_c - b\exp(-z_c/b)]}\right). \quad (2)$$

The ratio A_s/K (Equation 2) is an important parameter calculated in this study. The parameters in Equation 2 are derived as follows: T_C is the Curie temperature, which is taken as 580 °C (T_C of magnetite); T_S is the mean annual surface temperature, which is based on local climate stations and/or latitude and elevation (small errors in T_S are insignificant with respect to the uncertainty in T_C based on exact magnetic mineralogy); z_C is Curie depth, calculated from the spectral analysis of magnetic anomaly data (see Appendix A); $q_s = K(\mathrm{d}T/\mathrm{d}Z)_{z=0}$; and b is the depth parameter from the q_s-A_s relation. Substituting A_s/K and surface $(\mathrm{d}T/\mathrm{d}z)_{z=0}$ or A_s and $q_s = K(\mathrm{d}T/\mathrm{d}Z)_{z=0}$ in Equation 1, with the geotherm anchored at $T = T_c$ at $z = z_c$, T_z can be determined for all depths $z \leq z_c$.

If the analysis is restricted to provinces with major silicic plutons, as in this paper, then a reasonable assumption is that the upper crust is silicic in composition. All studies that make calculations of crustal geotherms must make assumptions of crustal thermal conductivities. Fortunately, the greatest variation in thermal conductivity is in quartz-bearing rocks in the uppermost crust. As the crust probably converges to a more intermediate and/or mafic composition with depth, and as crustal thermal conductivity decreases with increasing temperature, reasonable estimates of lower crustal conductivity may be made (Roy et al., 1981; Clauser and Huenges, 1995; Kukkonen et al., 1999). Thus, with a reasonable model of an average K for the crust, A_s may be calculated. Alternatively, if a reliable regional surface heat q_s is known, K may be determined from $q_s = K(\mathrm{d}T/\mathrm{d}z)$.

Application of the Method to Two Tectonically Diverse Regions in the United States with Radiogenic Heat-Production Data

In order to compare the results of our method and observations, we have identified two tectonically diverse regions in the United States where contributions from geology and/or tectonics may be deduced from geological and geophysical data sets. One is in New Hampshire, in the northeastern United States, where highly radiogenic granite batholiths in the upper crust contribute significantly to the geotherm and the temperatures are likely to be in steady state; the second is a boundary between the Archean Wyoming craton and tectonically younger northern Colorado.

New Hampshire

In central New Hampshire, we used the de-fractal method on the long-wavelength–corrected North American magnetic anomaly compilation known as NURE_NAMAM2008 (Ravat et al., 2009). Robustness of long wavelengths is important for the interpretation of deeper magnetic sources including the interpretation of Curie depths. We made three independent estimates of magnetic bottom (ranging from 25 to 32 km). Surface heat flow and its relationship to radiogenic heat production in the eastern United States is well established (Roy et al., 1968); the characteristic depth of heat-producing elements deduced from this is 7.5 km, and the reduced heat flow is 33 mW/m^2. In the Southern Methodist University heat-flow and/or thermal properties database (Blackwell and Richards, 2004), three heat-flow determinations in the region of the Conway granite are 79, 90, and 95 mW/m^2, and averages of hundreds of heat-production measurements from each of these locations are 7.36, 8.87, and 8.66 μW/m^3, respectively (Roy et al., 1968). The Conway granite covers a large area; it was emplaced during Mesozoic separation of North America from Europe (McHone and Butler, 1984) and is extremely rich in thorium (56 ± 6 ppm; Adams et al., 1962). Mean thermal conductivities of samples of rocks corresponding to the three heat-flow locations are 3.27, 3.56, and 3.7 W m^{-1} K^{-1} (Roy et al., 1968).

Following the details of the method shown in Appendix A, we show the de-fractal method's fractal parameter-corrected and modeled spectra for the New Hampshire example in Figure 1. The method relies on the consistency of magnetic top and bottom estimates from the forward-modeled and the de-

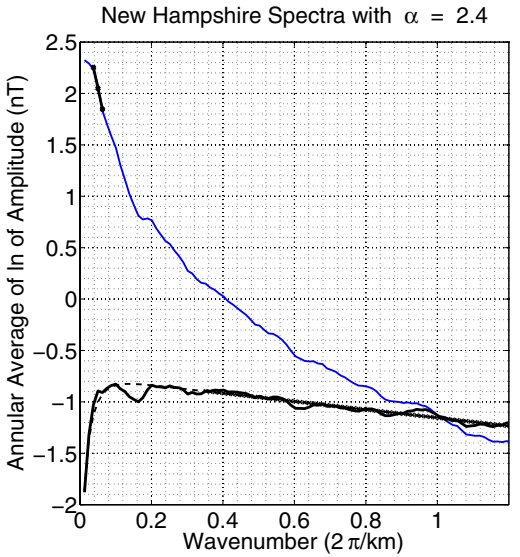

Figure 1. Spectra de-fractaled (bottom solid black curve) and modeled (black dashed curve) with the de-fractal method in New Hampshire, USA (Salem et al., 2014). See Appendix A and the Salem et al. (2014) reference for the description of how these estimates are derived. The magnetic bottom (Curie-depth) estimate in this case is 30 km. The de-fractal method (Salem et al., 2014) estimates the fractal parameter of the magnetic field and corrects the fractal nature of the observed spectra and compares it with the spectra from forward modeling with assumed 2-D fractal magnetization models. The method also relies on the consistency of estimates from the forward-modeling and the de-fractaled centroid method (based on the low wavenumber slope, i.e., slope of the solid black straight line in the low wavenumber part of the wavenumber scaled spectrum shown in blue in the upper part of the figure).

TABLE 1. RESULTS OF COMPUTATIONS OF SURFACE HEAT PRODUCTION (A_s) AND THERMAL CONDUCTIVITY (K) FROM NEW HAMPSHIRE BASED ON DERIVED A_s/K FROM EQUATION 2 FROM TWO VALUES OF CURIE DEPTHS

Input parameter	Parameter used to estimate thermal conductivity	Input parameter	Input parameter	Observation for comparison with the computed thermal conductivity	Output parameter	Observation for comparison with the computed surface heat production	Output parameter derived from A_s/K in Equation 2 and computed K
Curie-depth estimates (km)	Reduced heat flow used (mW/m^2)	Surface heat flow (mW/m^2)	Surface temperature (°C)	Observed average thermal conductivity (W m^{-1} K^{-1})	Computed thermal conductivity (W m^{-1} K^{-1})	Observed average surface heat production (μW/m^3)	Computed surface heat production, A_s (μW/m^3)
25	33	90	20	3.6	2.21	8.8	7.6
30	33	90	20	3.6	2.52	8.7	7.6

Note: Observed parameters from the Southern Methodist University data set on Conway granitic batholith and the results of our computations. Geotherms are derived from exponentially decreasing concentration of radiogenic elements in the crust with b of 7.5 km and reduced heat flow (q_r) of 33 mW/m^2 (Roy et al., 1968). Curie temperature of magnetite is 580°C.

fractaled centroid methods (see Salem et al., 2014). We used the Curie-constrained geotherm determination method on the New Hampshire heat-flow data, and the results are summarized in Table 1. We calculated unknown parameters (the ratio A_s/K) for a range of thermal conductivity values and selected values that closely match the known reduced heat flow in the region (Roy et al., 1968). Identifying K in this manner also determines A_s. These results show that where heat flow is steady state and the crustal heat production is relatively simple, observed average surface heat production and the calculated surface heat production (exponentially decreasing with depth) agree well.

The example shown in Figure 1 yielded a base of magnetization or Curie-depth estimate of 30 km. The Curie-depth–constrained geotherm and the geotherm computed using the observed radiogenic heat production from the Conway granite are similar and within the error bounds of the range of parameters used to construct them, as shown in Figure 2. More importantly, had one erroneously assumed a typical surface heat-production value of ~2 μW/m^3, which is often done in regions where heat production is not known, it would result in much lower temperatures in the crust and incorrect geophysical and geodynamical inferences (see continuous black geotherm with A_s of 2.1 μW/m^3 and K of 2.5 W m^{-1} K^{-1} in Fig. 2).

The derived high surface heat-production estimates give an approximate depth to the solidus of ~97–110 km (with mantle thermal conductivity value of 3.4 W m^{-1} K^{-1}), which is identical to the estimates of seismic lithosphere-asthenosphere boundary (LAB) from P to S (Ps) phase conversions at 97–110 km for this region (Rychert et al., 2005). However, the P to S (Ps) phase conversions from the nearby stations from which the interface was interpreted are the least clear and weakest among the data they had analyzed; and Rychert et al. (2007) suggest that it could be shallower than their 2005 study estimate. Regional anisotropy of seismic waves in the mantle and steep-dipping structure (Menke and Levin, 2002) could also introduce errors in the determinations. Nonetheless, the Curie depths derived in the study are consistent with seismic LAB determinations. Seismic LAB is controlled by factors such as composition, anisotropy, and water content, which are not identical to the factor that controls the thermal LAB (i.e., the solidus at a particular composition).

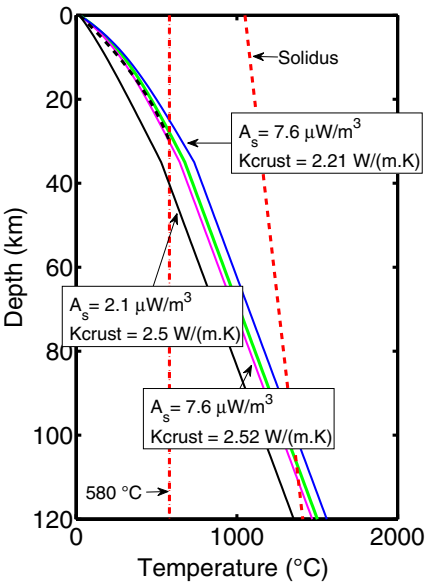

Figure 2. Steady-state one-dimensional geotherms for three different assumptions in New Hampshire, USA. The red dashed lines represent the 580 °C Curie temperature and the solidus with 3 °C/km. Curie-depth–constrained geotherms (magenta and blue solid geotherm lines) intersect the Curie temperature (580 °C) at the Curie depth (30 and 25 km, respectively) determined in this study from the de-fractal method. It is compared with the conventional geotherm computed with the observed surface radiogenic heat production of 8.7 μW/m^3 (green geotherm line). A mantle heat flow q_r = 33 mW/m^2 and the heat-production distribution parameter b = 7.5 km are used to constrain A_s/K, and these values are derived from the empirical linear relationship, $q_s = q_r + A_s b$, for the eastern United States (Roy et al., 1968). The thermal conductivity of mantle is assumed 3.4 W m^{-1} K^{-1}. The seismically observed lithospheric thickness is between 97 and 110 km depth in the region (Rychert et al., 2007) and thus is consistent with the Curie depths of 25–30 km. For comparison with the assumption of the exponential heat-production distribution, the assumption of the constant heat-production model with the Curie-depth–constraining approach leads to similar geotherm (black dash curve to 30 km depth) as the exponentially decreasing radiogenic heat-production model (magenta line with thermal conductivity of 2.52 Wm^{-1} K^{-1}) in this case. The parameters derived from the Curie temperature-depth–constraining approach for the constant heat-production model are: thermal conductivity, k = 3.27 W m^{-1} K^{-1} and the heat production, A = 1.93 μWm^{-3}; the input parameters were the same as in Table 1. If the high regional surface radiogenic heat production were not known and a typical value of heat production, e.g., 2.1 μWm^{-3} were assumed, as is often done in areas without heat-production estimates, one would obtain a geotherm shown in solid black line, which would significantly underestimate the temperatures throughout the lithosphere.

Northern Colorado to Wyoming Craton

The Wyoming block is an Archean cratonic core to which younger terranes were accreted (Whitmeyer and Karlstrom, 2007). Decker et al. (1988) have collected, compiled, and analyzed heat-flow, radiogenic heat generation, and conductivity measurements in Colorado and southern Wyoming. There is much variability over short distances in heat-flow observations in Colorado (64–140 mW/m^2; Decker et al., 1988, their table 3), and Decker et al. (1988) showed that the variability was related to upper crustal radiogenic heat-production variations (reaching values of up to 8–9 μW/m^3). In contrast, the Wyoming craton consists of once middle and lower crustal rocks lying presently in the upper part of the crust and thus explaining representative low radiogenic heat generation (1–2 μW/m^3) and low heat flow (<50 mW/m^2), except where there are rocks of granitic composition (Decker et al., 1988). Decker et al. (1988) synthesized their thermal data with interpretations of upper crustal granitic compositions from gravity lows (Brinkworth et al., 1968; Tweto and Case, 1972; Isaacson and Smithson, 1976; Johnson et al., 1984; Decker et al., 1988) to remove the upper crustal heat-production variability and called the resulting heat flow the residual heat flow. Using finite difference computations, they constructed crustal models of thermal parameters. Their models suggested near-solidus conditions for felsic compositions (~800 °C) near the bottom of the thickened crust in Colorado (Prodehl and Pakiser, 1980). The average upper crustal radiogenic heat generation for their models was 3.8 and 1–2.4 μW/m^3 for Colorado and Wyoming, respectively. In Decker et al.'s (1988) model, which is based on two seismic-refraction profiles between 105°W and 107°W longitudes (Jackson and Pakiser, 1965; Prodehl and Pakiser, 1980; see also Keller et al., 1998), a 10 km crustal thinning occurs from Colorado into Wyoming. However, joint analyses of the EarthScope seismic receiver function and gravity anomaly data show that the crustal thickness in both the regions is uniformly 45–55 km, and the average crustal V_p/V_s varies between 1.7 and 1.8, indicative of the bulk crustal composition from granites to diorites (Lowry and Pérez-Gussinyé, 2011). Similar high crustal thickness estimates in the Wyoming craton have also been derived in the recent work by Schmandt et al. (2015; digital results also presented in IRIS DMC, 2016). How these differences in Moho depth will influence the thermal model is difficult to judge because it depends on the distribution of heat-producing elements in the crust and whether the radiogenic elements extend all the way to the Moho or not. However, crossing the solidi alone in some regions would complicate the situation and modeling. To circumvent this issue, we compare the depth-integrated radiogenic heat production (which is the contribution of crustal radiogenic heat production to surface heat flow) between the model of Decker et al. (1988) and our results. Any advective heat or near-solidus temperatures in the affected parts of the crust will also reduce thermal conductivity (below 2 W m^{-1} K^{-1} at 800–1000 °C, Clauser and Huenges, 1995) and could reduce thermal conductivity for deep-seated rocks in the crust in comparison to the steady-state scenario modeled by Decker et al. (1988).

We calculated a large number of Curie depths at 125 km spacing in Colorado and the Wyoming craton (Fig. 3). Shallow Curie depths in this map generally correlate well with the areas of high surface heat flow (except where our 500 km spectral windows cannot capture the variation in the narrow zone in the Snake River Plain). The import of this regional correlation is that the spectral magnetic bottom estimates have no input from the heat flow or any other geophysical or geologic observations. The Curie depths in Colorado range between 22 and 32 km, with an average of ~26.5 km. Estimates in the Wyoming craton range between 24 and 52 km, with an average of 34 km. We calculated

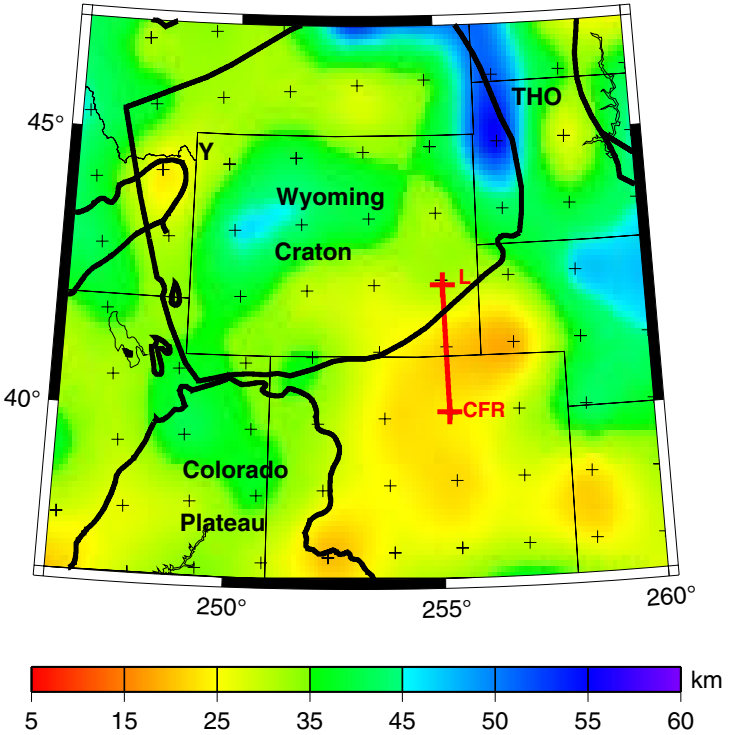

Figure 3. Curie-depth estimates from 500 km spectral windows (+) from the de-fractal method across the border of the Wyoming craton and the Colorado Front Range. Wyoming craton and Colorado Plateau are outlined in thick black line. Red line shows the profile of thermal properties shown in the next figure from Laramie (L) to Colorado Front Range (CFR) from Decker et al. (1988). In general, the Wyoming craton depth estimates are in the range of 34 ± 7.5 km and in the northern Colorado Plateau and eastward in Colorado, they are 26.5 ± 3.5 km. Along the Decker et al. (1988) profile, the transition between the two provinces appears to occur over roughly 60–70 km distance at the surface, which is reasonable for temperature variations expected in the lower crust. The de-fractal method with 500 km windows averages out the narrow-width uplifted geotherm in the Snake River Plain trailing the Yellowstone hotspot (Y). Trans-Hudsonian orogen (THO) is a 1.9–1.8 Ga suture zone between the Wyoming craton and the Superior craton to the east.

geotherms using the Curie-depth constraints at the end points of the crustal thermal parameters model profile of Decker et al. (1988), corresponding to the Laramie Range with Curie depth of ~30–33 km and surface residual heat flow of 45 mW/m^2, and the Colorado Front Range with Curie depth ~24–25 km, surface residual heat flow 85 mW/m^2. Using a radiogenic depth parameter, *b*, of 10 km, we first estimated the ratio A_s/K from Equation 2 and then varied the thermal conductivity to match the reduced heat-flow values of Decker et al. (1988) for the two provinces (30 and 20 mW/m^2, respectively, for Colorado and Wyoming). The results of these calculations are presented in Table 2.

Decker et al. (1988) used a three-layer crust model with different thermal parameters in each layer and a crustal boundary close to the Colorado-Wyoming state line (Fig. 4); in the figure, we show also the comparison between their and our geotherms. They did not have the benefit of a Curie-depth estimate in constructing their thermal model. For the Laramie Range region in Wyoming, our analysis yields temperatures in the lower crust ~200 °C hotter at the Curie depth than the Decker et al. (1988) models. The discrepancy between the two approaches arises primarily from two differences: First, Decker et al.'s (1988) thermal models have high middle and lower crustal radiogenic heat-production values and make the equivalent surface heat production in the exponentially decreasing formulation higher. The second difference is that the Wyoming craton crust is thicker than assumed by Decker et al. (1988) as previously discussed. Thus, it is possible the amount of radioactive elements may be greater in both these regions than estimated by Decker et al. (1988). Our (exponentially decreasing) surface radiogenic heat production in the Colorado Front Range is higher than the constant heat production of the upper layer in Decker et al. (1988), but our high values are compensating for high heat production of the middle crustal layer in the Front Range of Colorado used by Decker et al. (1988) (1 μW/m^3 higher than the corresponding layer in Wyoming). In the Wyoming craton, our magnetic bottom estimates (~34 km) are shallower than the Moho (except near the northeast edges of the craton), and therefore this magnetic bottom may correspond to the Curie depth. The mantle is often believed to be non-magnetic, and, if the Curie isotherm falls below the Moho, the bottom of magnetic sources is assumed to be the Moho (Wasilewski et al., 1979). The depth-integrated heat-production values (i.e., the contribution of crustal radiogenic heat production to surface heat flow) in Decker et al.'s (1988) model and our results are compared in the last two columns of Table 2, and they agree very well, showing that the Curie-depth constraint can yield reasonable bulk estimates for the crustal thermal parameters. The high surface radiogenic heat production values derived with the steady-state assumption could also be a reflection of magmatic heat in the lower crust in this case.

APPLICATION OF THE METHOD TO THE RED SEA REGION

In Salem et al. (2014), we used a similar method of Curie-depth–constrained geotherm modeling but with uniform radiogenic heat production (without derivations, albeit the same steps as in our derivation above) for deriving thermal parameters in the central Red Sea rift and the adjacent eastern and western margins. Our results from that study suggest that, in the central portion of the oceanic rift, where the Curie depth was only 6.4 km below the water depth (at the crust-mantle boundary at the window size of 100 km of that analysis), the temperature-depth profile was essentially linear. We do not have oceanic heat production measurements in this region, but the composition of the ocean crust at the mid-oceanic ridge can be assumed to be tholeiitic basalt and gabbro and the heat production somewhat uniformly low (<0.1 μW/m^3, Clauser, 2011). With the uniform heat-producing layer model and surface heat flow of 160 mW/m^2, surface temperature of 22 °C, and the Curie depth of 6.4 km below the ocean bottom (the parameters in Salem et al., 2014), we could only increase the average thermal conductivity in the Red Sea rift example to 1.83 W m^{-1} K^{-1}. This value is at the very low end of the range for silica-poor volcanic rocks (Clauser and Huenges, 1995) and possibly represents the effect

TABLE 2. PARAMETERS USED FROM THE MODEL OF VARIATION OF THERMAL CRUSTAL STRUCTURE BY DECKER ET AL. (1988) IN THE CURIE-CONSTRAINED GEOTHERM MODELS (SURFACE HEAT FLOW AND REDUCED HEAT FLOW) AND THE COMPUTED PARAMETERS

	Input parameter	Parameter used to estimate thermal conductivity	Input parameter	Output parameter	Output parameter	For comparison with the computed depth-integrated heat production	Output parameter derived from A_s/K in Equation 2 and computed *K*
Geologic province	Curie depth (km)	Reduced heat flow (mW/m^2)	Surface heat flow (mW/m^2)	Computed thermal conductivity (W m^{-1} K^{-1})	Computed surface heat production, A_s (μW/m^3)	Depth-integrated heat production contribution from the crustal column of Decker et al. (1988) model (mW/m^2)	Computed depth-integrated heat-production contribution from the crustal column (mW/m^2)
Colorado Front Range	24–25	30	85	2.15–2.2	5.5	60.0	55
Wyoming craton Laramie Range	30–33	20	45	1.5	2.5	26.5	25

Note: Geotherms are derived from exponentially decreasing concentration of radiogenic elements in the crust with *b* of 10 km. Since we do not have heat-production measurements from samples of rocks in this case, in the last two columns, we use the values of depth-integrated radiogenic heat generation (the contribution of crustal radiogenic heat production to surface heat flow) to compare Decker et al. (1988) results to ours.

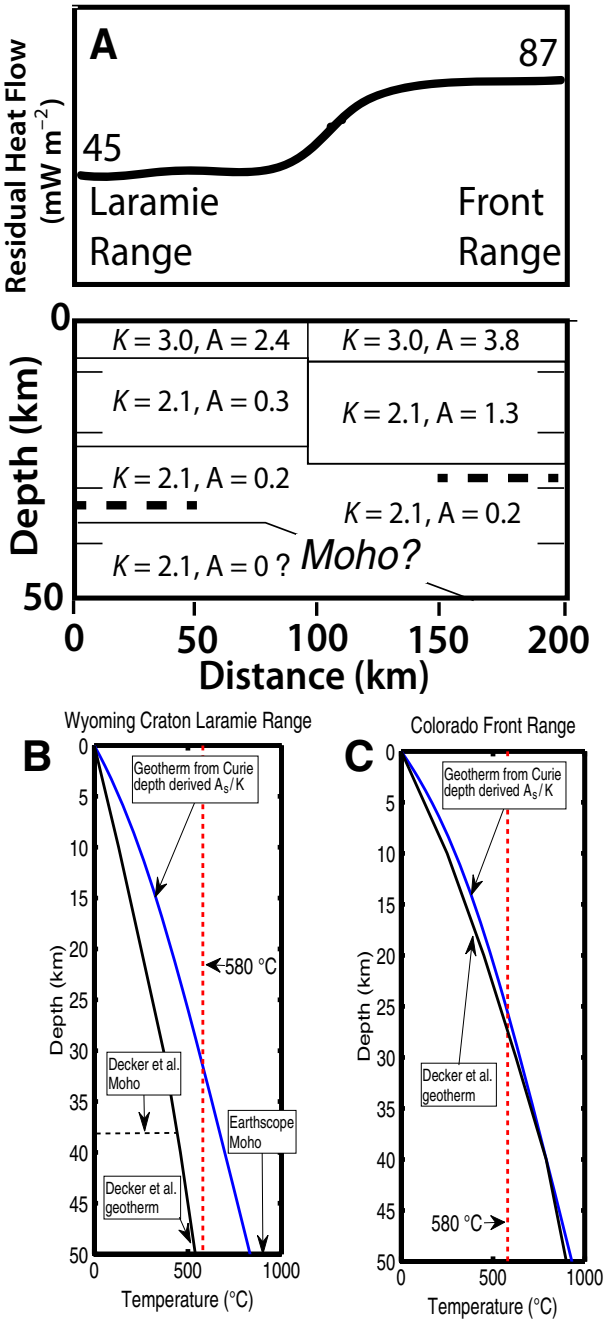

Figure 4. (A) Decker et al. (1988) thermal model for a profile from Colorado Front Range to Laramie Range, Wyoming (from north to south on the red line in Fig. 3). *K* is thermal conductivity in W m^{-1} K^{-1} and *A* is the heat production in μWm^3. Curie depths from the de-fractal method are shown with thick dashed lines. EarthScope receiver functions–based depths to the Moho are in the range of 45–55 km in both regions (Lowry and Pérez-Gussinyé, 2011; Schmandt et al., 2015; IRIS DMC, 2016). Based on the Curie depths, the location of transition from the Wyoming to Colorado provinces occurs in the northern part of the profile (toward Laramie Range) and not in the central portion as modeled by Decker et al. (1988); (B) and (C) Comparisons of geotherms from the Curie-constrained geotherm approach and the 2-D model of Decker et al. (1988). The input parameters, for the Curie-constrained geotherm computations, q_s, T_s, and *b*, are the same as given in Table 2 and its heading. The temperatures from the Curie-constrained geotherm approach are somewhat higher in the Colorado Front Range; and, in the Laramie Range, Wyoming, had the heat production of Decker et al. (1988) continued to the modern estimates of the Moho (~50 km), the discrepancy in geotherms from the two approaches would have been smaller.

of water-filled pore space in the uppermost section and reduction of thermal conductivity by higher temperatures in the lowermost mid-ocean ridge crust. The radiogenic heat production from this calculation was 0.14 μW/m^3, and the mantle heat flow was 159 mW/m^2. Radiogenic heat production for the layer is essentially negligible, consistent with the oceanic crust, leading to an approximately linear geotherm. When assuming different thermal conductivity (which means changing also the mantle heat flow), the derived ratio of A_s/K changes.

We do not have enough high-quality, long-wavelength magnetic data available in the coastal regions of either margin of the Red Sea to use 500 km windows as we did in the United States. Using the Curie depths obtained over the Saudi Arabian margin in the Salem et al. (2014) study (~17 km), the estimated surface heat production using the method of exponential heat production of this study (~1.7 μW/m^3) is consistent with the high end of measurements (1.46 ± 0.18 μW/m^3) by Gettings and Showail (1982), although the corresponding thermal conductivities obtained through both these analyses (1.3 W m^{-1} K^{-1}) is very low (assumed b = 10 km and q_r = 33 mW/m^2). Even increasing the Curie depth by 5 km (within the margin of error) and maintaining mantle heat flow at around 33 mW/m^2 does not increase thermal conductivity over 1.65 W m^{-1} K^{-1}. The interpretation of seismic refraction data 2°–3° south of this location does not suggest a great thickness of sediments (Healy et al., 1982; Mooney et al., 1985; Milkereit and Fluh,1985; Prodehl, 1985; Gettings et al., 1986), and only if the surface heat flow were higher than the 50 mW/m^2 assumed by Salem et al. (2014), or if the Curie depth were grossly underestimated due to the small window used in that study, could the conductivity approach 2 W m^{-1} K^{-1}. It is possible that the surface heat flow could be higher because the value of 50 mW/m^2 is based on a singular observation in the region (Rolandone et al., 2013), significantly distant from the magnetic anomaly window. It is important to note that these considerations are imposed by the lack of heat-flow data and uncertainties in the Curie depth due to a small window size rather than the method of constraining temperatures at depth for deriving the geotherm. Unfortunately, there are no heat-flow and thermal parameters available near the eastern margin to compare with our results on that margin.

CONCLUSION

We have developed a new method to incorporate a temperature-depth constraint in the solution of 1-D heat-flow equation for the geotherm. In this study, we use results of spectral analysis of magnetic anomaly data to derive the depth to the bottom of a magnetic layer, which can be associated with the Curie temperature of magnetite and, hence, yields a temperature-depth constraint in the crust. Used in conjunction with the Curie depth and surface heat flow, the method yields a geotherm anchored at the Curie depth and also a ratio of radiogenic heat production to thermal conductivity (A_s/K). Using the estimate of the mantle heat flow as a criterion (from the intercept of the regional surface heat-flow versus heat-production relationship), one can further constrain the range of A_s/K and K. If the resulting value of K is reasonable, then this method also can be used to deduce A_s (which is an important parameter for modeling the heat flow and often not measured in the field).

With the method outlined above, we obtained the Curie-depth–constrained geotherm and estimates of surface heat production (~8 μW/m^3) in New Hampshire, which are high but comparable to observed surface heat production values over the Conway granite in the region. This result validates the method for applications where steady-state heat-flow conditions apply. We also analyzed the region across the Archean Wyoming craton to Colorado where there is a transition from a low to a high heat-flow regime. The Curie-depth map also shows a variation across these domains from the Wyoming craton (Curie depths 24–52 km, with an average of 34 km) to northern Colorado (Curie depths of 22–32 km, with an average of 26.5 km). We compared our results of the Curie-depth–constrained geotherm modeling with the finite-difference models of thermal parameters by Decker et al. (1988). Our depth-integrated crustal heat-production values compared very well with the values of Decker et al. (1988) (see Table 2).

We also placed into perspective previous Curie-depth results of Salem et al. (2014) from the Red Sea (a profile from the western to the eastern margin). In that study, which was our first application of the Curie-depth–constraint technique (albeit with the uniform radiogenic heat production assumption), we obtained reasonable parameters for the heat production of the oceanic crust (close to zero) and thermal conductivities near the low end of the spectrum of the basaltic crust in high-temperature conditions. Inland from the Saudi Arabian margin of the Red Sea, we obtained heat-production values with our method, and these are consistent with the range of a few heat-production observations in the region.

In tectonothermally younger regions, when the estimated mantle heat flow is matched in these computations, the method appears to yield higher radiogenic heat generation values and lower thermal conductivity values than observations or estimates in the region (e.g., our Colorado and the central Red Sea examples). Despite this limitation, it appears that the method will prove useful in constraining geotherms and deriving heat-production estimates where steady-state situations apply. Temperature-depth constraints are also useful in deriving geotherms in transient temperature regimes with time-varying temperature-depth formulation (e.g., Wendlandt and Morgan, 1982; Morgan, 1983; Harrison et al., 1986; Lachenbruch et al., 1994), where steady-state assumptions would be inappropriate. We intend to carry out such computations in Sierra Nevada region in the near future.

ACKNOWLEDGMENTS

We are very grateful to Dr. Ahmed Salem for our interactions during the development of the de-fractal method. We thank the editors of *Geosphere*, reviewers (C. Bouligand, C. Buecker, and C. Gerbi), and Ms. Caitlyn Hartig for their comments, which improved the manuscript. Ms. Leah Newman's cross-checking of some of our spectral depth results is greatly appreciated. This research was funded by National Science Foundation grants EAR-1246921 to DR and EAR-1246977 to ARL.

APPENDIX A. SEMI-AUTOMATIZATION OF THE DE-FRACTAL METHOD OF SPECTRAL MAGNETIC DEPTH DETERMINATION

In the general procedure of Salem et al. (2014), the fractal parameter of the observed magnetic anomaly field is increased until there is consistency between depth estimates from the centroid method and the spectral peak modeling method. The procedure also requires determination of amplitude offset between the observed and modeled spectra for the peak modeling. The amplitude offset may be determined either manually or automatically by the least-squares fitting of the spectra. We have modified the procedure to make some of it interactive with some parts automatic such that in combination it results in more repeatable performance. The automation also allows us to examine a large number of solutions, in comparison to the manual approach, from which the best-fitting solutions can be selected manually and upper and lower bounds can be estimated from other equally well-fitting solutions. In the modified selection, we first fit the two amplitude (or power) spectra with the method of least squares and then readjust the fit by least-squares fitting the logarithm of amplitude (or power) over the range of wavenumbers selected on the basis of variations in the observed spectrum. The former method fits the peak region the best, and the latter fits better the overall curve of the amplitude spectrum over the selected wavenumber range. This process made the fit of the curves more comparable among different α. At the point of this writing, no mathematical misfit norm appeared to lead to the same selection as we might visually make because misfit functions minimize the difference between the observed and modeled curves, and as a result, the curves cross over in different segments (see Fig. A1a and the description below). On the other hand, for selecting correct depth to the bottom, we want to ensure that particular segments of the curves fit well without crossing over. We also tried several mathematical misfit norms (L2, L1, and L-infinity), but none could avoid the cross-over problem.

Based on model studies, repeatable and accurate estimates of the depth to the bottom are achieved routinely at a fractal parameter of the field (α) in the neighborhood of the one that leads to a minimum in the misfit. In Figure A1a, the spectra at the minimum root-mean-square (RMS) misfit between the observed and modeled spectral curves ($\alpha = 2.1$) from a model study are shown (where fractal parameter of magnetization β is 3; and so the fractal parameter of the field (α) should be close to 2; Maus and Dimri, 1994, for near-surface magnetic field data); one can observe cross-overs in the fit in the wavenumber range from 0 to 0.1—the key part of the curve for the depth to the bottom. Figure A1b shows the RMS misfit curve as a function of α. In the example shown, the fractal parameter at the RMS tightly hugs the left face of the peak; however, routinely, the best solutions are within ±0.2 of $\alpha_{\text{minimum misfit}}$. Another change in the software that improved the repeatability of our results is, instead of picking the centroid slope graphically (which led to different number of wavenumbers selected in different runs), determining the steepest centroid slope using a fixed number of consecutive wavenumber points (e.g., 2 or 3 points depending on the waviness of the curve right of the peak). Making sure that in the accepted solutions the slope of the de-fractaled centroid spectrum in the selected range is straight (and also not turned over due to de-fractalization) is also important.

Figure A2 shows the result of the model study for four models with different depths to the bottom of magnetization and the average and standard deviation of the results obtained with nine offset windows. The match is very good for a 500 km × 500 km window but results in underestimation of basal depths obtained from smaller window sizes (not shown to avoid clutter). In the figure, we also make comparisons with the approach of Li et al. (2013). They used automatically determined least-square slopes with preselected wavenumber ranges with the fractal parameter–

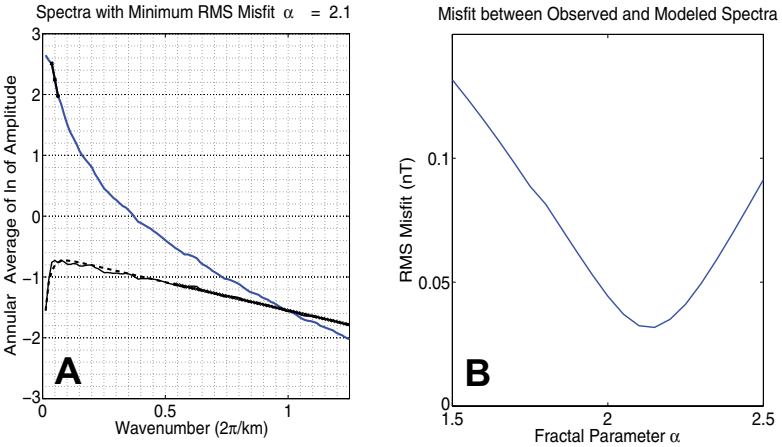

Figure A1. The de-fractal method of finding the base of magnetization. After applying the fractal correction, we estimate the depth to the top and the bottom of magnetic layer using the de-fractaled centroid method, where the blue spectrum at the top in (A) is the 1/wavenumber–scaled spectrum required in determining the depth to the centroid (Bhattacharyya and Leu, 1975; Okubo et al., 1985; Bansal et al., 2011). The solid black straight line is the straight slope selected for the centroid estimate. In the de-fractal method, we use the same de-fractal parameter to perform forward modeling of the observed de-fractaled spectrum with the modeled spectrum from the 2-D fractal magnetization model. The results shown are for a 40-km-thick layer with the observation plane of 1 km elevation above the depth to the top. The derived depth to the base of magnetization for this window is 39 km. (A) Comparison of the observed and modeled spectra (solid black line with the low wavenumber peak is the observed spectrum and the black dashed line is the modeled spectrum) showing the fit of the spectra at the minimum root mean square (RMS) difference between the observed and computed spectra (α = 2.1). ln—natural logarithm. (B) The RMS of the difference between observed and computed spectra against the fractal parameter of the field (α) used to compute the spectra. The selected solution hugs the left face of the peak of the de-fractaled spectrum but does not overfit or underfit the left face, and is generally close to the RMS minimum (but rarely identically at the RMS minimum).

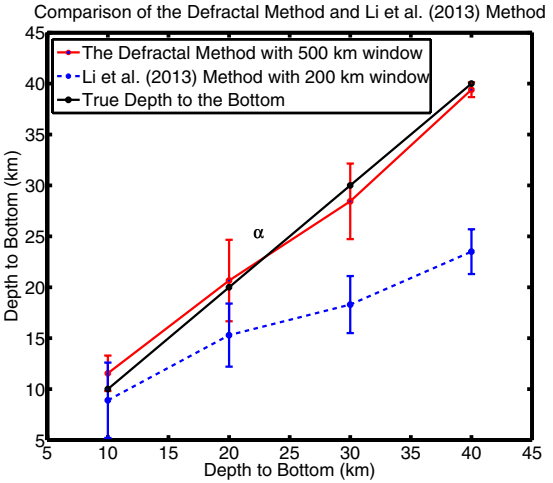

Figure A2. Comparison of the results from the de-fractal method (Salem et al., 2014, with improvements discussed in the appendix) with nine offset determinations of a 500 km window and Li et al. (2013) fractal correction centroid method of automatically picking depths from their recommendation of wavenumber range (from 81 realizations). Wavenumber range from which the centroid depths are picked changes, and it partly also depends on the behavior of the spectra and hence cannot be selected automatically; thus the method generally underestimates the depth to the base of magnetization. X-axis shows true depths and Y-axis shows computed depths for the spectral depth determinations. The results of the de-fractal method with 500 km window are superior. The de-fractal method does not perform well with smaller window sizes unless the depths to the bottom of are limited to 15–20 km from the observation windows. For the depths to the base of magnetization greater than 50 km, one would require much larger windows, which makes the analysis not very practical because the region of averaging may significantly smooth out the actual variation in the base of magnetization.

corrected centroid method (Bansal et al., 2011) to compute depths to top and bottom with small windows. Based on the results shown in Figure A2 and our experience with smaller windows, neither preselected wavenumber ranges nor small windows give consistent results.

During this study, we also developed a 3-D de-fractal approach where the fractal parameter of 3-D magnetization was iteratively estimated for each fractal parameter of the field being computed; however, the fractal parameters of the field and the magnetization may be dependent on each other, and consequently the misfit curve between observed and modeled spectra could not be used effectively in the selection of the solution. In model studies, the 2-D de-fractal method performed well on 3-D fractal magnetization distributions, and we attribute this primarily to the larger influence of layers near the top on the magnetic field than the layers at greater depth. Thus for all practical purposes, the magnetic field from a 3-D fractal crustal magnetization behaves as if it was generated by a 2-D fractal magnetization distribution.

APPENDIX B. JUSTIFICATION FOR USE OF THE EXPONENTIAL DISTRIBUTION OF HEAT PRODUCTION WITH DEPTH IN GRANITIC PLUTONS

The original papers introducing the linear heat-flow (Q)–heat-production (A) relation only claimed its application in major "granite" plutons and used these data to define "heat-flow provinces" (e.g., Birch et al., 1968; Roy et al., 1968). Lachenbruch (1968, 1970) introduced the proposal that heat production decreased exponentially with depth in these terrains in order to explain how the Q-A relation could survive differential erosion. He discussed how the heat-producing elements could be integrated in a vertical profile in a granitic pluton during melting. Lachenbruch also proposed a linear decrease in A with depth. This relation does not satisfy the condition of differential erosion, but it was within the error limits of the small data set of A versus depth available to Lachenbruch (1968). Other workers have extended the relation to mixed plutonic and/or metamorphic terranes or just metamorphic terranes. There is a general (statistical) Q-A linear relation in these terrains but of much poorer quality than the relation when applied to provinces with major "granite" plutons. There is no geochemical reason why the relation should be applicable to metamorphic terranes because the surface rocks in these terranes have no mechanism to be a representative "sample" of the upper crust.

Jaupart and Maraschal (2007) have claimed that there are no data to support the exponential model. Of the crustal sections that they cite, only two are granitic sections—the Vredefort structure and the Sierra Nevada (we exclude sections including metamorphic crust because they were not in the original definition of Q-A provinces and are not considered in this paper). If the data published for these sections are examined, the results are clearly indicative of weathered samples. Unweathered samples should have Th/U ratios of ~3.8–3.9 (Taylor and McLennan, 1985; Rocholl and Jochum, 1993) and K/U ratios of ~1–1.3 ± 0.3 × 10^4 (Taylor and McLennan, 1985; Rocholl and Jochum, 1993; Arevalo et al., 2009). Data published for the Vredefort structure (Nicolaysen et al., 1981) have Th/U and K/U ratios ranging from 4.7 to 24.4 (mean 15.5 ± 9.6, n = 14) and 1.0–14.9 × 10^4

(mean 6.3 ± 5.0 × 10^4, n = 14), respectively. Data published for the Sierra Nevada plutons (Brady et al., 2006) have Th/U and K/U ratios ranging from 0.1 to 91.7 (mean 6.6 ± 6.5, n = 57) and 0.3–12.5 × 104 (mean 2.1 ± 2.5 × 10^4, n = 57), respectively. These ranges of ratios are much greater and their means are far different from the bulk earth ratios expected for unweathered samples than ratio from borehole samples, e.g., from Decker et al. (1988): Th/U mean 4.4 ± 2.6 (n = 38) and K/U mean (1.0 ± 0.6) × 10^4 (n = 38).

Another indication that the samples from which the results presented by Brady et al. (2006) were probably weathered is that the mean heat production from these samples is 1.5 ± 1.2 μW/m^3 (n = 57), whereas the mean heat production from borehole samples reported by Saltus and Lachenbruch (1991) is 2.1 ± 1.1 μW/m^3 (n = 28). Although these means are not significantly different, the lower mean and larger standard deviation with the surface samples, although the sample size is larger, is what would be expected with weathered samples.

The analysis of the data presented above that have been used to "prove" that the exponential distribution is not valid demonstrates that samples used for the "proof" were probably weathered. Therefore the results from the surface samples from the Vredefort structure and the Sierra Nevada cannot be used to test the validity of the exponential distribution of heat production through the crust in granitic plutons.

The heat-flow data for the three test areas used in this paper are primarily from silicic plutons—the U.S. New England plutons, granitic plutons in northern Colorado and southern Wyoming in the United States, and plutons in the Saudi Arabian Shield adjacent to the Red Sea. Only New England is a well-defined heat-flow province because the other two areas are transitional heat-flow zones. Our analysis, as any model calculating crust geotherms, required an assumption of the distribution heat production with depth. As we have demonstrated above, there are no data invalidating the exponential distribution in major silicic plutons, and this distribution satisfies the documented observation of the linear Q-A relation with differential erosion in granitic pluton heat-flow provinces with high-quality heat-flow data. We do not claim that the distribution is valid in metamorphic terrains. One goal of the present study is to find and test temperature tie points deep in the crust that may be used to constrain crustal thermal parameters.

REFERENCES CITED

Adams, J.A.S., Kline, M.-C., Richardson, K.A., and Rogers, J.J.W., 1962, The Conway granite of New Hampshire as a major low-grade thorium resource: Proceedings of the National Academy of Sciences of the United States of America, v. 48, p. 1898–1905, doi:10.1073/pnas.48.11.1898.

Arevalo, R., McDonough, W.F., and Luong, M., 2009, The K/U ratio of the silicate Earth: Insights into mantle composition, structure and thermal evolution: Earth and Planetary Science Letters, v. 278, p. 361–369, doi:10.1016/j.epsl.2008.12.023.

Bansal, A.R., Gabriel, G., Dimri, V.P., and Krawczyk, C.M., 2011, Estimation of depth to the bottom of magnetic sources by a modified centroid method for fractal distribution of sources: An application to aeromagnetic data in Germany: Geophysics, v. 76, no. 3, p. L11–L22, doi:10.1190/1.3560017.

Bansal, A.R., Anand, S.P., Rajaram, M., Rao, V.K., and Dimri, V.P., 2013, Depth to the bottom of magnetic sources (DBMS) from aeromagnetic data of Central India using modified centroid method for fractal distribution of sources: Tectonophysics, v. 603, p. 155–161, doi:10.1016/j.tecto.2013.05.024.

Bhattacharyya, B.K., and Leu, L.K., 1975, Analysis of magnetic anomalies over Yellowstone National Park: Mapping the Curie-point isotherm surface for geothermal reconnaissance: Journal of Geophysical Research, v. 80, p. 4461–4465, doi:10.1029/JB080i032p04461.

Birch, F., Roy, R.F., and Decker, E.R., 1968, Heat flow and thermal history in New York and New England, *in* Zen, E., White, W.S., Hadley, J.B., and Thompson, Jr., J.B., eds., Studies of Appalachian Geology: New York, Interscience, p. 437–451.

Blackwell, D., and Richards, M., 2004, Geothermal Map of North America: American Association of Petroleum Geologists item 423, scale 1:65,000,000 (data files we obtained were available at http://smu.edu/geothermal. Presently data can be accessed at http://geothermal.smu.edu/gtda/ or another U.S. National Geothermal Data System node).

Bouligand, C., Glen, J.M.G., and Blakely, R.J., 2009, Mapping Curie temperature depth in the western United States with a fractal model for crustal magnetization: Journal of Geophysical Research, v. 114, B11104, doi:10.1029/2009JB006494.

Brady, R.J., Ducea, M.N., Kidder, S.B., and Saleeby, J.B., 2006, The distribution of radiogenic heat production as a function of depth in the Sierra Nevada batholith, California: Lithos, v. 86, p. 229–244, doi:10.1016/j.lithos.2005.06.003.

Brinkworth, G., Behrendt, J.C., and Popenoe, P., 1968, Geophysical investigations in the Colorado mineral belt: American Geophysical Union Transactions, v. 49, p. 668.

Carslaw, H.S., and Jaeger, J.C., 1986, Conduction of Heat in Solids: London, Oxford University Press, 510 p.

Clauser, C., 2011, Radiogenic heat production of rocks, *in* Gupta, H., ed., Encyclopedia of Solid Earth Geophysics: Dordrecht, The Netherlands, Springer, p. 1018–1024, doi:10.1007/978-90-481-8702-7_74.

Clauser, C., and Huenges, E., 1995, Thermal Conductivity of Rocks and Minerals: Rock Physics and Phase Relations: A Handbook of Physical Constants: American Geophysical Union, Reference Shelf, v. 3, p. 105–126, doi:10.1029/RF003p0105.

Decker, E.R., Heasler, H.P., Buelow, K.L., Baker, K.H., and Hallin, J.S., 1988, Significance of past and recent heat-flow and radioactivity studies in the Southern Rocky Mountains region: Geological Society of America Bulletin, v. 100, p. 1851–1885, doi:10.1130/0016-7606(1988)100<1851:SOPARH>2.3.CO;2.

Fowler, C.M.R., 2005, The Solid Earth: An Introduction to Global Geophysics (second edition): Cambridge, UK, Cambridge University Press, 684 p.

Gettings, M.E., and Showail, A, 1982, Heat-flow measurements at shot points along the 1978 Saudi Arabian seismic deep-refraction line, Part 1: Results of the measurements: U.S. Geological Survey Open-File Report 82-793, 102 p.

Gettings, M.E., Blank, H.R., Jr., Mooney, W.D., and Healey, J.H., 1986, Crustal Structure of Southwestern Saudi Arabia: Journal of Geophysical Research, v. 91, no. B6, p. 6491–6512, doi:10.1029/JB091iB06p06491.

Harrison, T.M., Morgan, P., and Blackwell, D.D., 1986, Constraints on the age of heating at the Fenton Hill site, Valles Caldera, New Mexico: Journal of Geophysical Research, v. 91, p. 1899–1908, doi:10.1029/JB091iB02p01899.

Healy, J.H., Mooney, W.D., Blank, H.R., Gettings, M.E., Kohler, W.M., Lamson, R.J., and Leone, L.E., 1982, Saudi Arabian seismic deep-refraction profile: Final project report: U.S. Geological Survey Open-File Report 02-37, 434 p.

IRIS DMC, 2016, Data Services Products: US-CrustVs-2015 model, Crust thickness and Crust and Uppermost mantle Vs model for the contiguous U.S., doi:10.17611/DP/EMCUSCRUSTVS2015.

Isaacson, L.B., and Smithson, S.B., 1976, Gravity anomalies and granite emplacement in west-central Colorado: Geological Society of America Bulletin, v. 87, p. 22–28, doi:10.1130/0016-7606(1976)87<22:GAAGEI>2.0.CO;2.

Jackson, W.H., and Pakiser, L.C., 1965, Seismic study of crustal structure in the Southern Rocky Mountains: U.S. Geological Survey Professional Paper 525-D, p. D-85–D-92.

Jaupart, C., and Maraschal, J.-C., 2007, Heat flow and thermal structure of the lithosphere, *in* Schubert, G., ed., Treatise of Geophysics: Oxford, UK, Elsevier, v. 6, p. 217–252.

Johnson, R.A., Karlstrom, K.E., Smithson, S.B., and Houston, R.S., 1984, Gravity profiles across the Cheyenne Belt, a Proterozoic suture in southeastern Wyoming: Journal of Geodynamics, v. 1, p. 445–472, doi:10.1016/0264-3707(84)90019-X.

Keller, G.R., Snelson, C.M., Sheehan, A.F., and Dueker, K.G., 1998, Geophysical studies of the crustal structure in the Rocky Mountain region: A review: Rocky Mountain Geology, v. 33, p. 217–228, doi:10.2113/33.2.217.

Kukkonen, I.T., Jokinen, J., and Seipold, U., 1999, Temperature and pressure dependencies of thermal transport properties of rocks: Implications for uncertainties in thermal lithospheric models and new laboratory measurements of high-grade rocks in the central Fennoscandian shield: Surveys in Geophysics, v. 20, p. 33–59, doi:10.1023/A:1006655023894.

Lachenbruch, A.H., 1968, Preliminary geothermal model of the Sierra Nevada: Journal of Geophysical Research, v. 73, p. 6977–6989, doi:10.1029/JB073i022p06977.

Lachenbruch, A.H., 1970, Crustal temperature and heat production: Implications of the linear heat-flow relation: Journal of Geophysical Research, v. 75, p. 3291–3300, doi:10.1029/JB075i017p03291.

Lachenbruch, A.H., Sass, J.H., and Morgan, P., 1994, Thermal regime of the southern Basin and Range Province: 2. Implications of heat flow for regional extension and metamorphic core complexes: Journal of Geophysical Research, v. 99, p. 22,121–22,133, doi:10.1029/94JB01890.

Li, C.-F., Wang, J., and Wang, T., 2013, Thermal evolution of the North Atlantic lithosphere: New constraints from magnetic anomaly inversion with a fractal magnetization model: Geochemistry, Geophysics, Geosystems, v. 14, p. 5078–5105, doi:10.1002/2013GC004896.

Lowry, A.R., and Pérez-Gussinyé, M., 2011, The role of crustal quartz in controlling Cordilleran deformation: Nature, v. 471, p. 353–357, doi:10.1038/nature09912.

Maus, S., and Dimri, V., 1994, Scaling properties of potential fields due to scaling sources: Geophysical Research Letters, v. 21, p. 891–894, doi:10.1029/94GL00771.

Maus, S., and Dimri, V., 1995, Potential field power spectrum inversion for scaling geology: Journal of Geophysical Research, v. 100, p. 12,605–12,616, doi:10.1029/95JB00758.
Maus, S., and Dimri, V., 1996, Depth estimation from the scaling power spectrum of potential fields?: Geophysical Journal International, v. 124, p. 113–120, doi:10.1111/j.1365-246X.1996.tb06356.x.
Maus, S., Gordon, D. and Fairhead, D., 1997, Curie-temperature depth estimation using a self-similar magnetization model: Geophysical Journal International, v. 129, p, 163–168, doi:10.1111/j.1365-246X.1997.tb00945.x
McEnroe, S.A., and Brown, L.L., 2000, A closer look at remanence-dominated aeromagnetic anomalies: Rock magnetic properties and magnetic mineralogy of the Russell Belt microcline-sillimanite gneiss, northwest Adirondack Mountains, New York: Journal of Geophysical Research, v. 105, p. 16,437–16,456, doi:10.1029/2000JB900051.
McHone, J.G., and Butler, J.R., 1984, Mesozoic igneous provinces of New England and the opening of the North Atlantic Ocean: Geological Society of America Bulletin, v. 95, p. 757–765, doi:10.1130/0016-7606(1984)95<757:MIPONE>2.0.CO;2.
Menke, W., and Levin, V., 2002, Anomalous seaward dip of the lithosphere-asthenosphere boundary beneath northeastern USA detected using differential-array measurements of Rayleigh waves: Geophysical Journal International, v. 149, p. 413–421, doi:10.1046/j.1365-246X.2002.01652.x.
Milkereit, B., and Fluh, E.R., 1985, Saudi Arabia refraction profile: Crustal structure of the Red Sea–Arabian Shield transition: Tectonophysics, v. 111, p. 283–298, doi:10.1016/0040-1951(85)90289-6.
Mooney, W.D., Gettings, M.E., Blank, H.R., and Healy, J.H., 1985, Saudi Arabian seismic deep-refraction profile: A traveltime interpretation of crustal and upper mantle structure: Tectonophysics, v. 111, p. 173–246, doi:10.1016/0040-1951(85)90287-2.
Morgan, P., 1983, Constraints on rift thermal processes from heat flow and uplift: Tectonophysics, v. 94, p. 277–298, doi:10.1016/0040-1951(83)90021-5.
Nicolaysen, L.O., Hart, R.J., and Gale, N.H., 1981, The Vredefort radioelement profile extended to supracrustal strata at Carletonville, with implications for continental heat flow: Journal of Geophysical Research, v. 86, p. 10,653–10,661, doi:10.1029/JB086iB11p10653.
Okubo, Y., Graf, R.J., Hansen, R.O., Ogawa, K., and Tsu, H., 1985, Curie point depths of the island of Kyushu and surrounding areas, Japan: Geophysics, v. 50, p. 481–494, doi:10.1190/1.1441926.
Pilkington, M., and Todoeschuck, J.P., 1993, Fractal magnetization of continental crust: Geophysical Research Letters, v. 20, p. 627–630, doi:10.1029/92GL03009.
Pilkington, M., and Todoeschuck, J.P., 1995, Scaling nature of crustal susceptibilities: Geophysical Research Letters, v. 22, p. 779–782, doi:10.1029/95GL00486.
Prodehl, C., 1985, Interpretation of a seismic-refraction survey across the Arabian Shield in western Saudi Arabia: Tectonophysics, v. 111, p. 247–282, doi:10.1016/0040-1951(85)90288-4.
Prodehl, C., and Pakiser, L.C., 1980, Crustal studies of the southern Rocky Mountains from seismic measurements: Geological Society of America Bulletin, v. 91, p. 147–155, doi:10.1130/0016-7606(1980)91<147:CSOTSR>2.0.CO;2.
Ravat, D., Pignatelli, A., Nicolosi, I., and Chiappini, M., 2007, A study of spectral methods of estimating the depth to the bottom of magnetic sources from near-surface magnetic anomaly data: Geophysical Journal International, v. 169, p. 421–434, doi:10.1111/j.1365-246X.2007.03305.x.
Ravat, D., Finn, C., Hill, P., Kucks, R., Phillips, J., Blakely, R., Bouligand, C., Sabaka, T., Elshayat, A., Aref, A., and Elawadi, E., 2009, A preliminary, full spectrum, magnetic anomaly grid of the United States with improved long wavelengths for studying continental dynamics—A website for distribution of data: U.S. Geological Survey Open-File Report 2009-1258, 2 p.
Robinson, P., Harrison, R.J., McEnroe, S.A., and Hargraves, R.B., 2002, Lamellar magnetism in the haematite-ilmenite series as an explanation for strong remanent magnetization: Nature, v. 418, p. 517–520, doi:10.1038/nature00942.
Rocholl, A., and Jochum, K.P., 1993, Th, U and other trace elements in carbonaceous chondrites: Implications for the terrestrial and solar-system Th/U ratios: Earth and Planetary Science Letters, v. 117, p. 265–278, doi:10.1016/0012-821X(93)90132-S.
Rolandone, F., Lucazeau, F., Leroy, S., Mareschal, J.-C., Jorand, R., Goutorbe, B., and Bouquerel, H., 2013, New heat flow measurements in Oman and the thermal state of the Arabian Shield and Platform: Tectonophysics, v. 589, p. 77–89, doi:10.1016/j.tecto.2012.12.034.
Ross, H.E., Blakely, R.J., and Zoback, M.D., 2006, Testing the use of aeromagnetic data for the determination of Curie depth in California: Geophysics, v. 71, p. L51–L59, doi:10.1190/1.2335572.
Roy, R.F., Blackwell, D.D., and Birch, F., 1968, Heat generation of plutonic rocks and continental heat flow provinces: Earth and Planetary Science Letters, v. 5, p. 1–12, doi:10.1016/S0012-821X(68)80002-0.
Roy, R.F., Beck, A.E., and Touloukian, Y.S., 1981, Thermophysical properties of rocks, *in* Touloukian, Y.S., Judd, W.R., and Roy, R.F., eds., Physical Properties of Rocks and Minerals: New York, McGraw-Hill, p. 409–502.
Rychert, C.A., Fischer, K.M., and Rondenay, S., 2005, A sharp lithosphere-asthenosphere boundary imaged beneath eastern North America: Nature, v. 436, p. 542–545, doi:10.1038/nature03904.
Rychert, C.A., Rondenay, S., and Fischer, K.M., 2007, P-to-S and S-to-P imaging of a sharp lithosphere-asthenosphere boundary beneath eastern North America: Journal of Geophysical Research, v. 112, no. B08314, doi:10.1029/2006JB004619.
Salem, A., Green, C., Ravat, D., Singh, K.H., East, P., Fairhead, J.D., Mogren, S., and Biegert, E., 2014, Depth to Curie temperature across the central Red Sea from magnetic data using the de-fractal method: Tectonophysics, v. 624–625, p. 75–86, doi:10.1016/j.tecto.2014.04.027.
Saltus, R.W., and Lachenbruch, A.H., 1991, Thermal evolution of the Sierra Nevada: Tectonic implications of new heat flow data: Tectonics, v. 10, p. 325–344, doi:10.1029/90TC02681.
Schmandt, B., Lin, F.-C., and Karlstrom, K.E., 2015, Distinct crustal isostasy trends east and west of the Rocky Mountain Front: Geophysical Research Letters, v. 42, p. 10290–10298, doi:10.1002/2015GL066593.
Spector, A., and Grant, F.S., 1970, Statistical models for interpreting aeromagnetic data: Geophysics, v. 35, p. 293–302, doi:10.1190/1.1440092.
Tanaka, A., Okubo, Y., and Matsubayashi, O., 1999, Curie point depth based on spectrum analysis of magnetic anomaly data in East and Southeast Asia: Tectonophysics, v. 306, p. 461–470, doi:10.1016/S0040-1951(99)00072-4.
Taylor, S.R., and McLennan, S.M., 1985, The Continental Crust: Its Composition and Evolution: Oxford, UK, Blackwell, 312 p. (see p. 47).
Tweto, O., and Case, J.E., 1972, Gravity and magnetic features as related to geology in the Leadville 30-minute quadrangle, Colorado: U.S. Geological Survey Professional Paper 726-C, 31 p.
Wasilewski, P.J., Thomas, H.H., and Mayhew, M.A., 1979, The Moho as a magnetic boundary: Geophysical Research Letters, v. 6, p. 541–544, doi:10.1029/GL006i007p00541.
Wendlandt, R.F., and Morgan, P., 1982, Lithospheric thinning associated with rifting in East Africa: Nature, v. 298, p. 734–736, doi:10.1038/298734a0.
Whitmeyer, S.J., and Karlstrom, K.E., 2007, Tectonic model for the Proterozoic growth of North America: Geosphere, v. 3, p. 220–259, doi:10.1130/GES00055.1.
Wollenberg, H.A., and Smith, A.R., 1987, Radiogenic heat production of crustal rocks: An assessment based on geochemical data: Geophysical Research Letters, v. 14, p. 295–298, doi:10.1029/GL014i003p00295.